Original Article

Institution of MECHANICAL ENGINEERS
Journal of ENGINEERING TRIBOLOGY

Proc IMechE Part J:
J Engineering Tribology
0(0) 1–15

DOI: 10.1177/1350650118806377
journals.sagepub.com/home/pij
SAGE

Stability analysis of a rigid rotor supported by two-lobe hydrodynamic journal bearings operating with a non-Newtonian lubricant

Saurabh K Yadav[1], Arvind K Rajput[2], Nathi Ram[3] and Satish C Sharma[4]

Abstract

In the present work, an investigation has been performed on a rigid rotor supported by two-lobe journal bearings operating with a non-Newtonian lubricant. The governing Reynolds equation for pressure field is solved by using non-linear finite element method. Further to study the dynamic stability of the bearing system, governing equation of motion for the rotor position is solved by fourth order Runge–Kutta method. Bifurcation and Poincaré maps of two-lobe bearings are presented for different values of the non-Newtonian parameter and bearing ellipticity ratio. The numerical results illustrate that the ellipticity of a bearing with a dilatant lubricant improve the stability of the rotordynamic system.

Keywords

Rotordynamic stability, bifurcation diagram, vibration, offset ratio, non-Newtonian lubricant

Date received: 12 April 2018; accepted: 19 September 2018

Introduction

The performance of a rotating machine mainly depends upon the performance of the bearing system. Hydrodynamic journal bearings are widely used in different rotatory machineries in industries due to its inherent characteristics to avoid direct metal-to-metal contact and support heavy load in rotating machines with lesser friction. Hydrodynamic journal bearings not only support heavy load but also provide high value of stiffness and damping coefficient to rotor system. Damping and stiffness of these bearings mainly depend on the fluid film profile of the bearing and behavior of the lubricant. Damping and stiffness coefficients of the bearing play a key role in the dynamic response of a rotor. Therefore, it is necessary to investigate the dynamic performance of the bearing and its influence on the behavior of a machine.

Generally, rotor bearing systems experience unbalanced harmonic force due to eccentricity, unbalance mass, misalignment of rotational masses and manufacturing errors. Such repeating harmonic forces result in chaotic motion of journal and make the machine unsafe and unstable. Hence, it becomes obvious to investigate the dynamic behavior of machine under such conditions.

In the past, various studies[1–4] have been conducted to analyze the dynamic response of the bearing. Adileta et al.[1] presented the effect of bearing conditions that gives rise to chaotic motion in a bearing. They theoretically analyzed the chaotic motion by using the numerical integration of equation of motion. Bifurcation plot were presented to visually analyze the dynamic behavior of a bearing for the applied condition.[2,3] They performed a number of numerical trials to find the system's chaotic responses. They also compared the theoretical results with the experimental data. Wang and Chen[4] performed the study on the dynamic analysis of a rotor bearing

[1]Department of Mechanical Engineering, Institute of Infrastructure, Technology, Research and Management (IITRAM), Gujarat, India
[2]Department of Mechanical Engineering, Shiv Nadar University, Greater Noida, India
[3]Department of Mechanical and Automation Engineering, IGDTUW, New Delhi, India
[4]Mechanical and Industrial Engineering Department, Indian Institute of Technology Roorkee, Roorkee, India

Corresponding author:
Saurabh K Yadav, Department of Mechanical Engineering, Institute of Infrastructure, Technology, Research and Management (IITRAM), Gujarat, India.
Email: saurabhme.iitr@gmail.com

supported by the aerodynamic gas film bearing. Their results indicate that rotor mass and rotational velocity significantly influence the dynamic behavior of the rotor system. They presented journal trajectories, power spectra, Poincare map and bifurcation map. Jian and Chens[5] presented the bifurcation and chaos study of a flexible rotor bearing system. Their study illustrates that the dynamic study of the system includes 2T-periodic, quasi-periodic and chaotic motions. They also discussed the existence of a complex rotordynamic behavior indicating periodic and sub-harmonic responses of the rotor center.

Wang et al.[6] studied the gas journal bearing system with herringbone-grooved by considering a rigid rotor[6] and a flexible rotor.[7,8] Their study illustrates the complex dynamic behavior of the rotor bearing system indicating periodic and quasi-periodic responses. Yang et al.[9] presented a new nonlinear dynamic analysis method of rotor system. They used second order approximation to evaluate the oil film stiffness and damping coefficients of the bearings. They presented nonlinear dynamic performance of a symmetrical flexible rotor-bearing system via the journal orbit and Poincaré map. Chen and Yau[10] studied the chaos in the flexible rotor supported by the oil film bearing by using fractal dimension concept. They suggested that the critical fluid film-bearing system operate in a chaotic region. Piekos[11] simulated the gas lubricated journal bearings for microfabricated machines by using orbit formulation method. They developed two numerical tools for orbit formulation. Non-linear bifurcation theory was used to predict stable or unstable periodic oscillations close to the critical speed. Chouchane and Amamou[12] applied numerical continuation to obtain stable or unstable limit cycles bifurcation from the equilibrium point at the critical speed.

Weimin et al.[13] presented a numerical method to compute the linear dynamic coefficient of journal bearings by using partial derivative method. They applied a small perturbation method on the oil film thickness which results in perturbation of the oil film pressure. By using a dynamic oil film pressure, they computed static and dynamic coefficients of the oil film journal bearing.

The dynamic response of the bearing strongly depends upon the fluid film pressure distribution and fluid film distribution significantly depends on the circularity of bearing. Therefore, various analyses have been performed on the noncircular bearing.[14,15] Meybodi et al.[14] used finite element method to solve Reynolds equation and fourth order Runge–Kutta method was used to solve dynamic equations. They illustrated the nonlinear dynamic behavior of the system by using periodic, KT-periodic and quasi-periodic responses of the rotor center.

To enhance lubricating performance, certain types of additives are generally blended with the lubricant. The addition of additives significantly affects the behavior of the lubricant and the lubricant no longer follow the Newton law of viscosity.[16,17] The additized lubricant are usually modeled by power law lubricant. Therefore, several studies carried out to study the influence of non-Newtonian power law lubricant on the dynamic response of the bearing system. Sharma and Yadav[18] studied that nonlinear behavior on the dynamic performance of hydrostatic/hybrid thrust bearing. They considered pseudo-plastic and dilatant behavior of the lubricant for their analysis. Sharma and Kushare[17] investigated the nonlinear behavior of the lubricant for a two-lobe hydrostatic journal bearing operating with the non-Newtonian lubricant. Their study indicates that a judicious selection of surface roughness and bearing geometry is essential for the stability of the bearing system.

From the study of the available literature on rotor bearing systems, it is found that no study shows the combined influence of offset factor and non-Newtonian nature of the lubricant on the dynamics of the system. Therefore, the present study is aimed to investigate the influence of a non-Newtonian lubricant on the dynamic response of rotors supported by two-lobe bearings as shown in Figure 1(a). The present study indicates that bearing behavior is basically depending on the four parameters viz. journal speed, fluid film thickness profile, journal mass and non-Newtonian parameter. The bifurcation diagrams are plotted by taking mass and journal speed as system variables. It is expected that result will contribute significant advancement in the development of the rotor bearing system having a non-Newtonian lubricant.

Analysis

The analysis of a two-lobe fluid film bearing operating with non-Newtonian lubricants performed with the following assumptions:

1. Lubricant in the bearing clearance is assumed to be isothermal. Temperature in the fluid film bearing is constant.
2. The non-Newtonian behavior of the lubricant is modeled by using power law model of the lubricant.
3. The side leakage of the flow is negligible.

The governing Reynolds equation in a non-dimensional form for the non-Newtonian lubricant in the clearance space of a two-lobe bearing in Figure 1(b) is written as follows[16,17,19–22]

$$\frac{\partial}{\partial\alpha}\left(\bar{h}^{3}\bar{F}_{2}g\frac{\partial\bar{p}}{\partial\alpha}\right)+\frac{\partial}{\partial\beta}\left(\bar{h}^{3}\bar{F}_{2}g\frac{\partial\bar{p}}{\partial\beta}\right)=\Lambda_{\mathrm{cav}}\bar{U}\left(1-\frac{F_{1}}{F_{0}}\right)\frac{\partial\bar{h}}{\partial\alpha}+a_{cav}\frac{\partial\bar{h}}{\partial\tau} \tag{1}$$

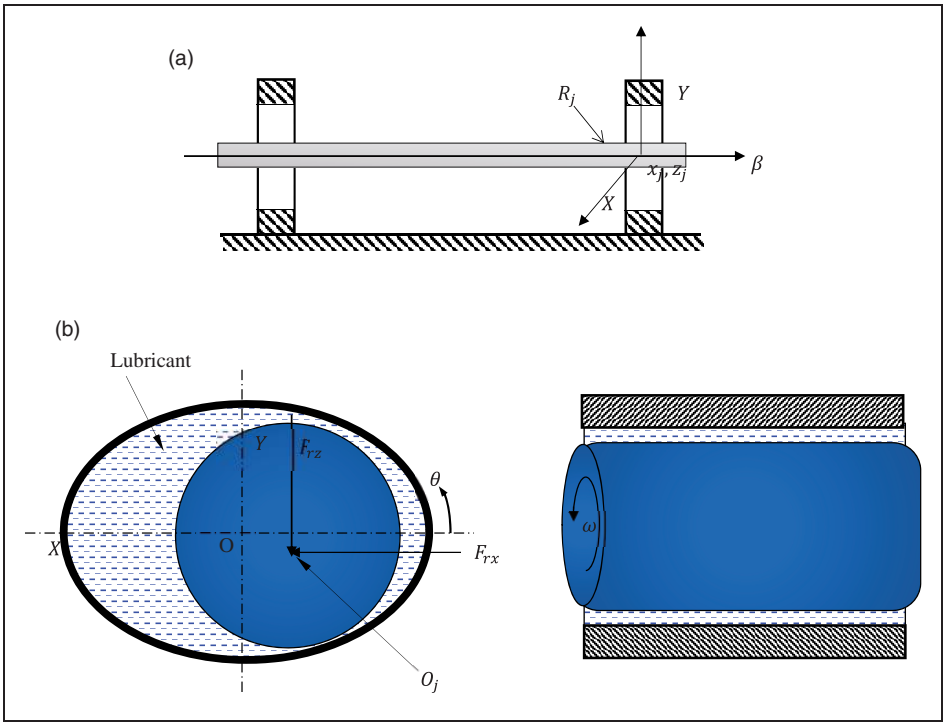

Figure 1. Schematic diagram of (a) rotor bearing system and (b) two-lobe journal bearing.

where the non-dimensional parameters are $\bar{p} = \frac{p}{p_s}$, $\bar{h} = \frac{h}{C_r}$, $\bar{u} = \frac{R\omega}{P_a}\left(\frac{R}{C}\right)^2$, $\alpha = \frac{x}{R}$, $\beta = \frac{y}{R}$, $\tau = \omega t$.

where $\bar{F}_0$, $\bar{F}_1$ and $\bar{F}_2$ are the cross apparent viscosity integrals used for the non-Newtonian lubricant. The computation of these integral is carried out as follows

$$\bar{F}_0 = \int_0^1 \frac{1}{\bar{\mu}} \mathrm{d}\bar{z}, \quad \bar{F}_1 = \int_0^1 \frac{\bar{z}}{\bar{\mu}} \mathrm{d}\bar{z}, \\ \bar{F}_2 = \int_0^1 \frac{\bar{z}}{\bar{\mu}} \left(\bar{z} - \frac{\bar{F}_1}{\bar{F}_0}\right) \mathrm{d}\bar{z} \tag{2a}$$

In this work, power law model of a lubricant is used to obtain the shear stress and shear strain relationship and it is mathematically represented as follows[16,23]

$$\bar{\tau} = \left(\bar{\dot{\gamma}}\right)^k \tag{2b}$$

Fluid film thickness

The fluid film thickness of a two-lobe bearing is calculated by using following expression[17,24]

$$\bar{h} = 1 - \left(\bar{x}_j - \bar{x}_l\right)\sin(\theta) - \left(\bar{z}_j - \bar{z}_l\right)\cos(\theta) \\ + \left(1 - \frac{1}{\delta}\right)\cos\left(\theta - \theta_l^k\right) \tag{3}$$

where $\bar{x}_l, \bar{z}_l$ are the coordinate of the lobe centre and θ_l^k is the lobe angle.

Finite element analysis

To obtain the stiffness and damping coefficient for the two-lobe bearing solution of Reynolds equation is required but the solution of Reynolds of a non-Newtonian lubricant cannot be done by using close form solution. Therefore, a nonlinear finite element method (FEM) has been implemented in the present work to compute stiffness and damping coefficient of the rotor bearing system. The finite element discretization of the fluid film domain in unwrapped and wrapped forms is indicated in Figure 2(a) and (b), respectively. The fluid film pressure variation over an element is computed as[25,26]

$$\bar{p} = \sum_{j=1}^{n_l^e} p_j N_j \tag{4}$$

Applying the orthogonality conditions of Gallerkin's technique of FEM, the following finite element matrix is obtained.[27]

$$\left[\bar{F}_{ij}\right]^e \{\bar{p}\}^e = \{\bar{Q}_i\}^e + \Omega\{\bar{R}_{Hi}\}^e + \bar{\dot{X}}_J\{\bar{R}_{X_J i}\}^e + \bar{\dot{Z}}_j\{\bar{R}_{Z_J i}\}^e \tag{5}$$

Global system of equation for Reynolds equation is expressed as[28]

$$\left[\bar{F}\right]_{n\times n}\{\bar{p}\}_{n\times 1} = \{\bar{Q}\}_{n\times 1} + \Omega\{\bar{R}_H\}_{n\times 1} \\ + \bar{\dot{X}}_J\{\bar{R}_{X_J}\}_{n\times 1} + \bar{\dot{Z}}_J\{\bar{R}_{Z_J}\}_{n\times 1} \tag{6}$$

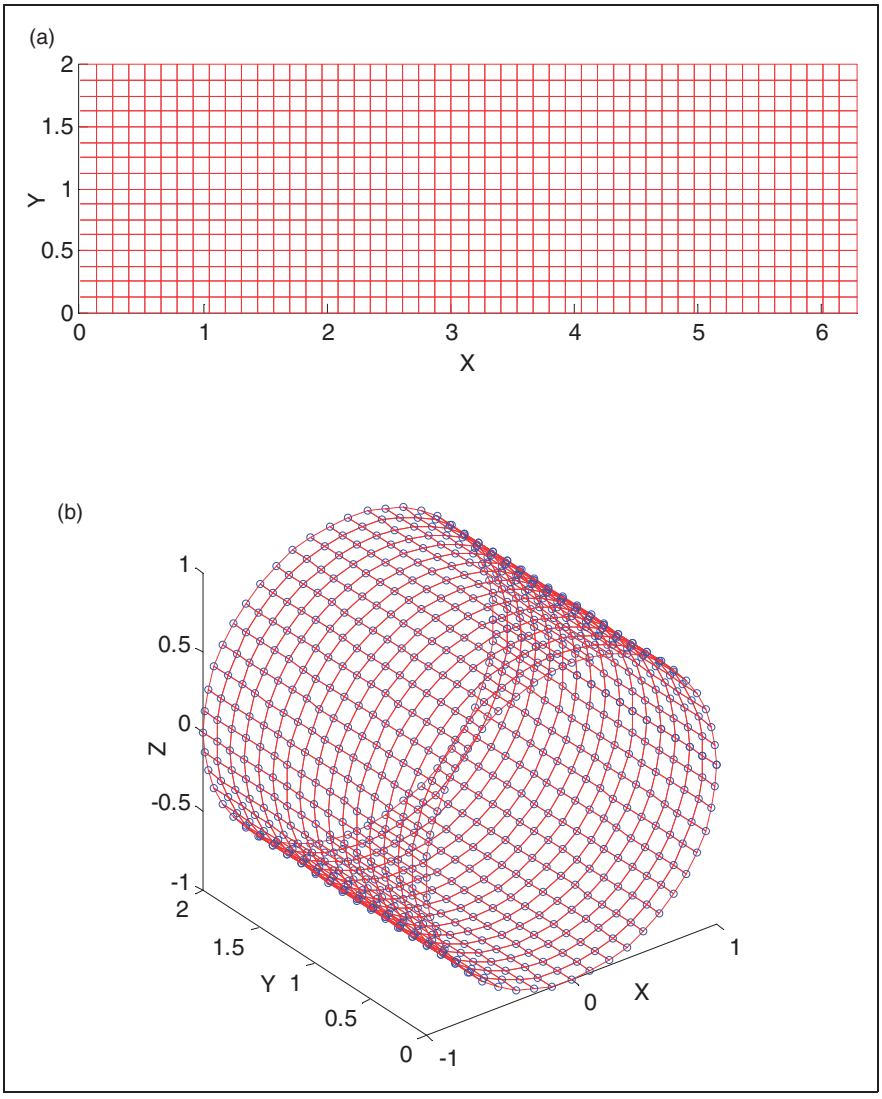

Figure 2. Finite element mesh of two-lobe hydrodynamic journal bearing (a) unwrapped surface, (b) (wrapped surface).

Bearing performance parameter

To evaluate the dynamic performance of bearing, the computation of the fluid film stiffness and damping coefficient is required. The fluid film stiffness and damping coefficient of a two-lobe journal bearing are computed as following.[29]

Fluid film stiffness coefficients. The fluid film stiffness coefficients are calculated as

$$S_{ij} = -\frac{\partial \bar{F}_i}{\partial q_j} \quad (i = x, z) \tag{7}$$

where "i" represents the direction of force and q_j represents the displacement of journal center coordinate ($\bar{x}_j$ or $\bar{z}_j$).

The four components of stiffness and damping coefficient are computed as follows

$$\bar{S}_{xx} = -\frac{\partial \bar{F}_{rx}}{\partial \bar{x}_j} = -\int_{-1}^{1}\int_{0}^{2\pi} \frac{\partial \bar{p}}{\partial \bar{x}_j}\cos\alpha \mathrm{d}\alpha \mathrm{d}\beta \tag{8a}$$

$$\bar{S}_{zx} = -\frac{\partial \bar{F}_{rz}}{\partial \bar{x}_j} = -\int_{-1}^{1}\int_{0}^{2\pi} \frac{\partial \bar{p}}{\partial \bar{x}_j}\sin\alpha \mathrm{d}\alpha \mathrm{d}\beta \tag{8b}$$

$$\bar{S}_{xz} = -\frac{\partial \bar{F}_{rx}}{\partial \bar{z}_j} = -\int_{-1}^{1}\int_{0}^{2\pi} \frac{\partial \bar{p}}{\partial \bar{z}_j}\cos\alpha \mathrm{d}\alpha \mathrm{d}\beta \tag{8c}$$

$$\bar{S}_{zz} = -\frac{\partial \bar{F}_{rz}}{\partial \bar{z}_j} = -\int_{-1}^{1}\int_{0}^{2\pi} \frac{\partial \bar{p}}{\partial \bar{z}_j}\sin\alpha \mathrm{d}\alpha \mathrm{d}\beta \tag{8d}$$

Fluid film damping coefficients. The fluid film damping coefficients are defined as

$$C_{ij} = -\frac{\partial \bar{F}_i}{\partial \dot{q}_j} \quad (i = x, z) \tag{9}$$

$\dot{q}_j$ represents the velocity component of journal center in $\dot{x}_j$ or $\dot{z}_j$ directions.

The components of damping coefficient matrix are computed as

$$\bar{C}_{xx} = -\frac{\partial \bar{F}_{rx}}{\partial \dot{\bar{x}}_j} = -\int_{-1}^{1}\int_{0}^{2\pi} \frac{\partial \bar{p}}{\partial \dot{\bar{x}}_j}\cos\alpha \mathrm{d}\alpha \mathrm{d}\beta \tag{10a}$$

$$\bar{C}_{zx} = -\frac{\partial \bar{F}_{rz}}{\partial \dot{\bar{x}}_j} = -\int_{-1}^{1}\int_{0}^{2\pi} \frac{\partial \bar{p}}{\partial \dot{\bar{x}}_j}\sin\alpha \mathrm{d}\alpha \mathrm{d}\beta \tag{10b}$$

$$\bar{C}_{xz} = -\frac{\partial \bar{F}_{rx}}{\partial \dot{\bar{z}}_j} = -\int_{-1}^{1}\int_{0}^{2\pi} \frac{\partial \bar{p}}{\partial \dot{\bar{z}}_j}\cos\alpha \mathrm{d}\alpha \mathrm{d}\beta \tag{10c}$$

$$\bar{C}_{zz} = -\frac{\partial \bar{F}_{rz}}{\partial \dot{\bar{z}}_j} = -\int_{-1}^{1}\int_{0}^{2\pi} \frac{\partial \bar{p}}{\partial \dot{\bar{z}}_j}\sin\alpha \mathrm{d}\alpha \mathrm{d}\beta \tag{10d}$$

Boundary conditions

The boundary conditions are suitably applied in the bearing model on the basis of available study in the literature.

1. To avoid cavitation, the Reynolds boundary conditions have been used $\left(\bar{p} = \frac{\partial \bar{p}}{\partial \alpha} = 0\right)$.
2. All the nodes lying on the external boundary has been assigned zero relative pressure with respect to atmospheric pressure ($p_{Boundary=\pm 1} = 0$).

Dynamic stability analysis

The following assumptions are considered to analyze the dynamics of a rotor bearing system.

i. The rotor mass and bearing mass are lumped at the midpoint.
ii. The effect of axial and torsional vibrations is negligible.
iii. Shaft and rotor disk is considered as massless.
iv. The rotor, bearing and the support of bearing are radially symmetric.

The governing equation of motion for the rotor bearing system is expressed in equation (11). The behavior of equation of motion is nonlinear; therefore, equation (11) for a small time step (Δt) is expressed as[30]

$$\left[\mathbf{M}_r\right]\left\{\ddot{\bar{\mathbf{X}}}_J\right\} + \left[\mathbf{C}\right]\left\{\dot{\bar{\mathbf{X}}}_J\right\} + \left[\mathbf{S}\right]\left\{\mathbf{X}_J\right\} = \left[\bar{F}_r\right] \tag{11}$$

The above equation of motion can be written in matrix form as

$$\begin{bmatrix} \bar{M}_r & 0 \\ 0 & \bar{M}_r \end{bmatrix}\begin{Bmatrix} \ddot{\bar{x}}_j \\ \ddot{\bar{z}}_j \end{Bmatrix} + \begin{bmatrix} \bar{C}_{xx} & \bar{C}_{xz} \\ \bar{C}_{zx} & \bar{C}_{zz} \end{bmatrix}\begin{Bmatrix} \dot{\bar{x}}_j \\ \dot{\bar{z}}_j \end{Bmatrix} + \begin{bmatrix} \bar{S}_{xx} & \bar{S}_{xz} \\ \bar{S}_{zx} & \bar{S}_{zz} \end{bmatrix}\begin{Bmatrix} \bar{x}_j \\ \bar{z}_j \end{Bmatrix} = \begin{Bmatrix} \bar{m}_r\bar{\rho}\bar{\omega}^2\sin(\varphi) \\ \bar{m}_r\bar{\rho}\bar{\omega}^2\cos(\varphi) \end{Bmatrix} \tag{12}$$

To solve the above equation, state space model has been developed. Further developed state space model has been solved by using fourth order Rung–Kutta method.[31]

$$[\mathbf{X}] = \begin{bmatrix} \bar{x}_j \\ \bar{z}_j \\ \dot{\bar{x}}_j \\ \dot{\bar{z}}_j \end{bmatrix}, \quad [\dot{\mathbf{X}}] = \begin{bmatrix} \dot{\bar{x}}_j \\ \dot{\bar{z}}_j \\ \ddot{\bar{x}}_j \\ \ddot{\bar{z}}_j \end{bmatrix} \tag{13}$$

These are computed as

$$\dot{\mathbf{X}} = \mathrm{f}(\mathbf{X}) \tag{14a}$$

$$\mathbf{k}_1 = \mathrm{f}(\mathbf{X}_i) \tag{14b}$$

$$\mathbf{k}_2 = \mathrm{f}\left(\mathbf{X}_i + \mathbf{k}_1 \times \frac{\Delta t}{2}\right) \tag{14c}$$

$$\mathbf{k}_3 = \mathrm{f}\left(\mathbf{X}_i + \mathbf{k}_2 \times \frac{\Delta t}{2}\right) \tag{14d}$$

$$\mathbf{k}_4 = \mathrm{f}(\mathbf{X}_i + \mathbf{k}_3 \times \Delta t) \tag{14e}$$

After computing coefficients $\mathbf{k}_1$, $\mathbf{k}_2$, $\mathbf{k}_3$ and $\mathbf{k}_4$, the updated positions and journal centre velocities are calculated as

$$\mathbf{X}_{i+1} = \mathbf{X}_i + \left(\frac{\mathbf{k}_1 + 2\mathbf{k}_2 + 2\mathbf{k}_3 + \mathbf{k}_4}{6}\right) \times \Delta t \tag{15}$$

The parameter X_i is used to plot trajectory, chaotic diagram and bifurcation plots from the solution.

Solution scheme

Implementation of the above solution requires an iterative procedure, because the viscosity of a non-Newtonian lubricant cannot be computed. Therefore, a solution scheme has been built to get the bifurcation map and chaotic motion of bearing. The solution procedure shown in Figure 3 has been implemented in the following steps.

1. Mesh generation of fluid domain in four node elements as shown in Figure 2.
2. Initialization of all initial conditions of the fluid film pressure and fluid film derivative.
3. For values of the fluid film pressure, fluid film pressure derivative with respect to $\dot{\bar{x}}_j$, $\dot{\bar{z}}_j$ and fluid film pressure derivative with respect to $\bar{x}_j$, $\bar{z}_j$ are initialized.
4. Generation of gauss points in elemental domain for the integration of equations (8) and (9).

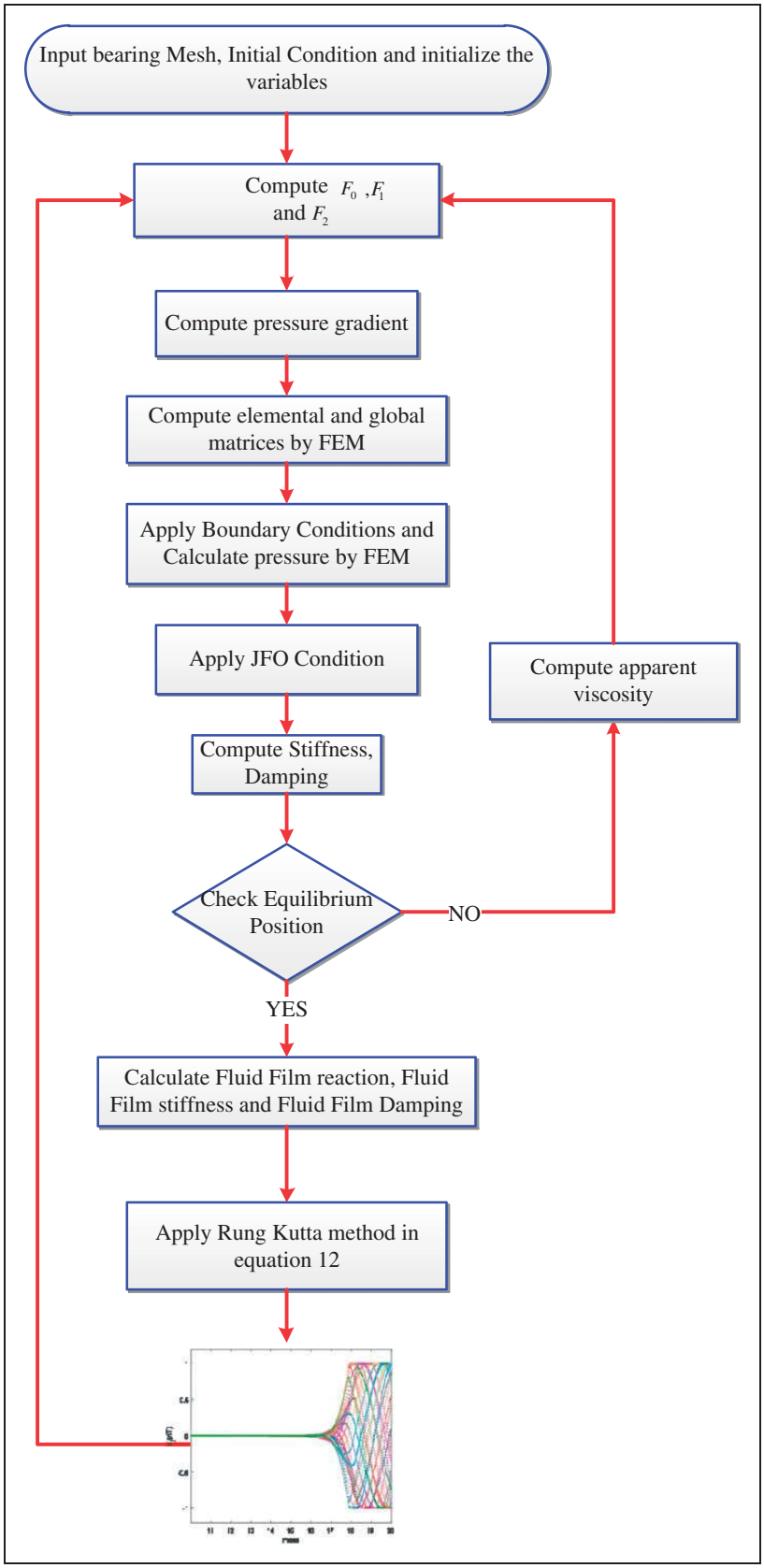

Figure 3. Solution algorithm flow chart.

5. Assemble element matrix into global system of equation.
6. Apply boundary condition in the global system of equation for pressure.
7. Applying Newton Raphson method, the fluid film pressure matrix is computed by solving the linearized system of equation.
8. Update the new pressure by taking the weighted average as follows

$$\{\bar{p}\}_{new} = (1-w)\{\bar{p}\}_{old} + w\{\bar{p}\}_{Computed} \tag{16}$$

where w is weighted average and it has the value between 0 and 1.

9. Check the convergence of the fluid film pressure and journal center position.
10. Check the following convergence criteria for equilibrium position

$$\frac{\left(\left((\bar{x}_j)_{i+1} - (\bar{x}_j)_i\right)^2 + \left((\bar{z}_j)_{i+1} - (\bar{z}_j)_i\right)^2\right)}{(\bar{x}_j)^2_{i+1} + (\bar{z}_j)^2_{i+1}} < 0.0001 \tag{17}$$

11. Compute stiffness and damping coefficient by using the derivative of fluid film pressure derivative with respect to $\overline{\dot{x}_j}$, $\overline{\dot{z}_j}$ and fluid film pressure derivative with respect to $\bar{x}_j$, $\bar{z}_j$.
12. Once, all the convergence criteria are satisfied, program finalizes the solution for an unknown fluid film pressure field.
13. Apply Rung–Kutta method for next time step and go to step 4.
14. Plot the bifurcation diagram, Poincare map of the motion.

Results and discussion

On the basis of the mathematical analysis and solution procedure discussed in earlier sections, a MATLAB program has been developed to examine the dynamic response of a rotor supported by a two-lobe bearing operating with power law lubricant. To authenticate the methodology adopted, the present results have been compared for the circular bearing and two-lobe bearing operating with a Newtonian lubricant. Table 1 indicates a comparison of results of the circular bearing with published results by Rehmatabadi et al.[32] for the chosen values of bearing operating and geometric parameter. A good agreement between the present and the published results may be observed from Table 1. The maximum error in the obtained results and the published results is 3.58%. Further, the present results are validated for the two-lobe bearing having twin groove used by Lund and Thomson[33,34] as indicated in Table 2. The maximum error observed in the simulated results is 5%. To get the confidence with finite element mesh, a convergence study has been performed by using finite element mesh. In Figure 4, eccentricity has been plotted as a function of load. The result of finite element converges as we increase the mesh size. The results show that 900 nodes in finite element produce results with good accuracy. Figure 5 shows the

Table 2. The present result and Lund and Thomson.[33,34]

Parameter	Present work	Lund and Thomson[30,31]
Eccentricity (ε_0)	0.10544	0.100
Fluid film stiffness $\left(\frac{\bar{S}_{xx}}{\bar{F}_z}\right)$	0.4126	0.24
Fluid film stiffness $\left(\frac{\bar{S}_{xz}}{\bar{F}_z}\right)$	10.5601	10.79
Fluid film stiffness $\left(\frac{\bar{S}_{zx}}{\bar{F}_z}\right)$	−11.002	−11.25
Fluid film stiffness $\left(\frac{\bar{S}_{zz}}{\bar{F}_z}\right)$	18.5067	18.93
Fluid film damping $\left(\frac{\bar{C}_{xx}}{\bar{F}_z}\right)$	9.4136	9.40
Fluid film damping $\left(\frac{\bar{C}_{xz}}{\bar{F}_z}\right)$	12.8750	12.97
Fluid film damping $\left(\frac{\bar{C}_{zx}}{\bar{F}_z}\right)$	12.9862	12.97
Fluid film damping $\left(\frac{\bar{C}_{zz}}{\bar{F}_z}\right)$	37.1336	38.73

Table 1. The present result and Rehmatabadi et al.[32]

Eccentricity ratio	Present result (load carrying capacity)	Multiplication factor	Present result with multiplication factor (load carrying capacity)	Rehmatabadi et al.[32] (load carrying capacity)	% Error
0.1	0.52	0.5	0.26	0.251	3.586
0.2	1.011	0.5	0.5055	0.501	0.898
0.4	2.36	0.5	1.18	1.175	0.426
0.6	5.058	0.5	2.529	2.54	0.433
0.8	13.136	0.5	6.168	6.152	0.260
0.9	28.963	0.5	14.4815	15.045	0.422

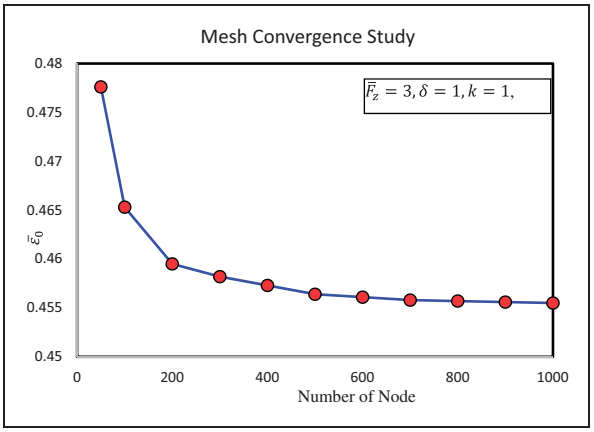

Figure 4. Mesh convergence study.

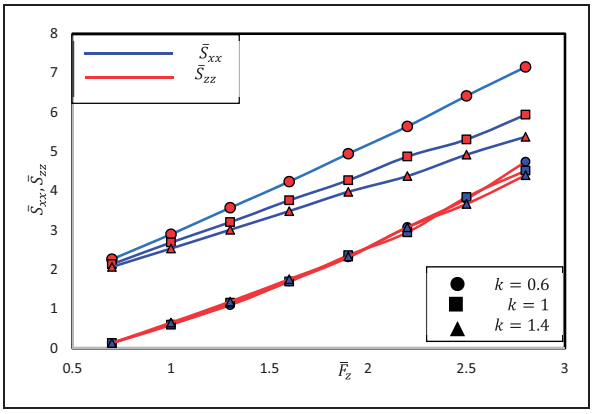

Figure 5. Fluid film stiffness coefficient variation with load.

variation of the fluid film stiffness coefficient with applied load.

In order to examine the dynamic behavior of a rotor bearing system, the dynamic trajectories of journal center plotted. These trajectories enable to distinguish whether the system is periodic or non-periodic but not provide adequate information about the chaos, i.e. motion is either of quasi periodic, periodic or chaotic. Poincare map and bifurcation diagram characterize the chaotic behavior of a rotor bearing system. A Poincare section is a hyper surface in state space transverse to the flow of the system. The points on Poincare section indicate the return points of the time series at a constant interval T (driving period of exciting force). The projection of Poincare section on $\bar{x}_j(NT) - \bar{z}_j(NT)$ is termed as Poincare map of journal dynamics. The return points in Poincare map form a closed curve for quasi-periodic motion. For chaotic motion, the return points form a particular structure or many irregular points while for NT-periodic motion, return points are N discrete points.

Bifurcation diagram is an effective method to characterize the non-linear behavior of any dynamic system. In a rotor bearing system, the non-linearities in dynamic behavior may exists due to either of rotor speed and rotor mass.[35] Therefore, the bifurcation

Table 3. Parameters used for a two-lobe journal bearing.[7,9,21,25,28,33]

Bearing parameters	Value
Bearing diameter (D)	50 mm
Bearing length (L)	50 mm
Radius clearance (c)	50 μm
Offset ratio (c)	0.7,1,1.3
Atmospheric pressure (P_a)	1.01325×10^5 Pa
Lubricant viscosity (η)	0.0028 N·s/m^2
Lubricant density (ρ)	850 Kg/m^3
r/min of journal	2000–5000 r/min
Non-Newtonian parameter (k)	0.5, 0.7, 1, 1.3, 1.5
Eccentricity (ρ)	0 to 0.8
Number of lobe	2

diagrams have been plotted by taking rotor speed ratio and mass ratio as system variables individually. To generate a bifurcation diagram, the system variable (speed ratio or mass ratio) is varied with a constant step and the state variables at the end of one integration step are used as the initial value for the next step. The operating and geometric parameter of bearing has been judiciously chosen on the basis of available literature and indicated in Table 3. In the present study, the time step size is $\pi/200$. The time series data of the first 20,000 time steps are excluded from dynamic behavior investigation. The results are presented for different values of non-Newtonian parameter and offset ratio.

Effect of bearing ellipticity parameter

The stability of a bearing is greatly affected by offset ratio of two-lobe bearing. Therefore, to examine the effect of bearing ellipticity parameter on the stability of a rotor bearing system operating with a Newtonian lubricant, bifurcation maps are plotted with speed ratio and mass and indicated in Figures 6 and 7 respectively. A significant change in the stability of the bearing is recorded by changing the bearing offset ratio. For the bearing having $\delta = 0.7$, the magnitude of dynamic motion of $\bar{x}_j(nT)$ and $\bar{z}_j(nT)$ is noted from -1 to 1 in local bifurcation whereas this magnitude of dynamic motion of $\bar{x}_j(nT)$ and $\bar{z}_j(nT)$ is from -0.8 to 0.8. Figure 6 represents the bifurcation diagrams of rotor center in horizontal and vertical direction for different values of ellipticity parameters ($\delta = 0.7, 1.0, 1.3$). It may be noticed that Figure 6 represents the stability of a rotor bearing system. In bifurcation map, location of the journal has been plotted for various cycles and each cycle is represented with a different color. It may be noticed from Figure 6 that the bifurcation of the rotor centre takes place in the speed range of $1 < \bar{\omega}$. The chaotic motion of rotor bearing system having ellipticity ratio (δ) of 0.7 is observed for $2.5 < \bar{\omega}$. Whereas the chaotic motion

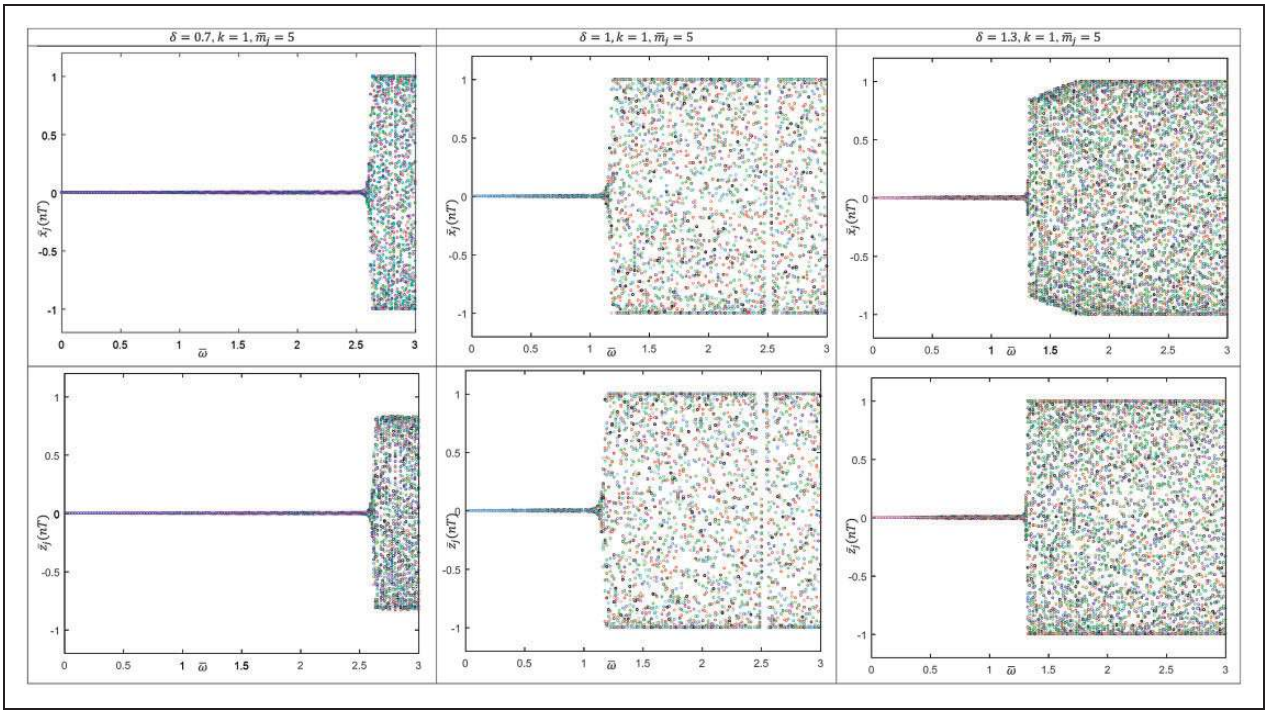

Figure 6. Bifurcation diagram of two-lobe bearing by taking $\bar{\omega}$ as a system variable.

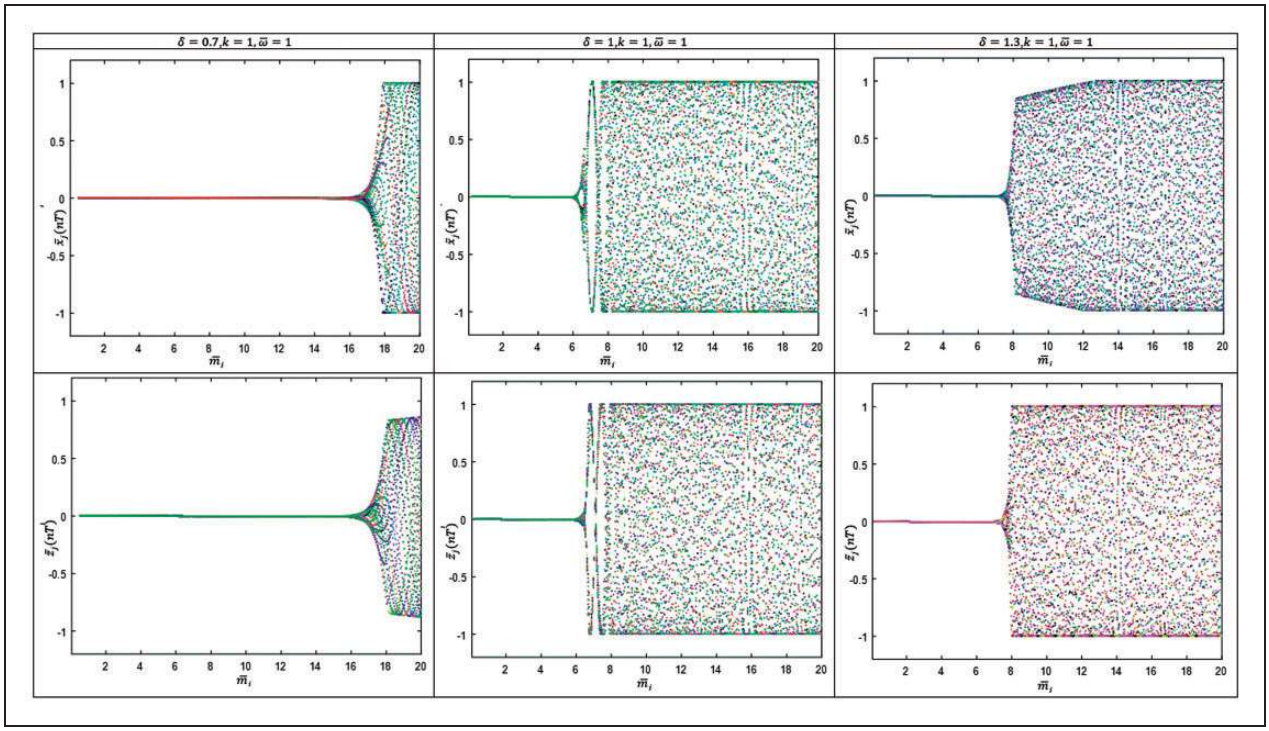

Figure 7. Bifurcation diagram of two-lobe bearing circular bearing by taking mass as a system variable.

of rotor bearing system having ellipticity ratio (δ) of 1 is observed for $1 < \bar{\omega}$ and the chaotic motion of rotor bearing system having ellipticity ratio (δ) of 1.3 is observed for $1.2 < \bar{\omega}$. The stability of the bearing can be characterized on the basis of journal speed ratio. Similarly, in Figure 7, bifurcation map has been presented by taking rotor mass as a system parameter. From the bifurcation map of bearing system, the system behavior can easily be observed, where the rotor bearing system having ellipticity ratio (δ) of 0.7 shows a stable behavior in motion for $17 > \bar{m}$. The location of after n cycles can be observed with different colored points. Whereas the rotor bearing system having ellipticity

ratio (δ) of 1 and 1.3 becomes unstable for $6.5 < \bar{m}$. From bifurcation map shown in Figures 6 and 7, it may be observed that the stability of the rotor bearing system is function of journal speed, ellipticity ratio and journal mass.

A Poincaré map is an effective way to represent state of a dynamical system with reduced dimensions. It is often used for analyzing the original dynamical system in a simpler way. Therefore, a Poincaré map has been shown in Figure 8 for different masses and bearing ellipticity for rotor bearing motion. A stable motion has been recorded for $k = 1, \bar{m} = 5, \bar{\omega} = 1$ at all values of ellipticity ratios ($\delta = 0.7, 1.0, 1.3$). Whereas unstable dynamic periodic motions have been observed at $k = 1, \bar{\omega} = 1$ and $\bar{m} = 10$ for elliptical bearing with $\delta = 1, 1.3$ whereas a stable dynamic periodic motion is observed with $\delta = 0.7$. Hence, it can be said that if the offset is less than 1, the two-lobe bearing is more stable. Figure 8 indicates that the change in the mass of the system results in a change in the stability of the system.

Effect of non-Newtonian parameter

The addition of additives in the lubricant makes the lubricant non-Newtonian. Shear stress and strain behavior of these Newtonian lubricants is represented as dilatant ($k>1$) and pseudo-plastic ($k<1$) lubricant. This non-Newtonian behavior of lubricants significantly affects the stability of the rotor bearing system. Therefore, to examine the effect of the non-Newtonian lubricant on the dynamics of rotor bearing system, bifurcation diagrams are plotted with speed ratio and mass ratio and indicated in Figures 9 and 10, respectively. Therefore, bifurcation diagram has been plotted in Figure 9 for various value of power law index. The bifurcation diagram in Figure 9 has been plotted with rotor centre displacement ($\bar{x}_j, \bar{z}_j$) against the non-dimensional rotor mass ($\bar{m}$). The different behavior has been observed for the selected values of $\bar{m}$. For the pseudo-plastic lubricant ($k = 0.7$), the bearing shows the bifurcation of the rotor centre for the speed range of $\bar{m} < 7$. For the Newtonian lubricant ($k = 1$), the two-lobe bearing

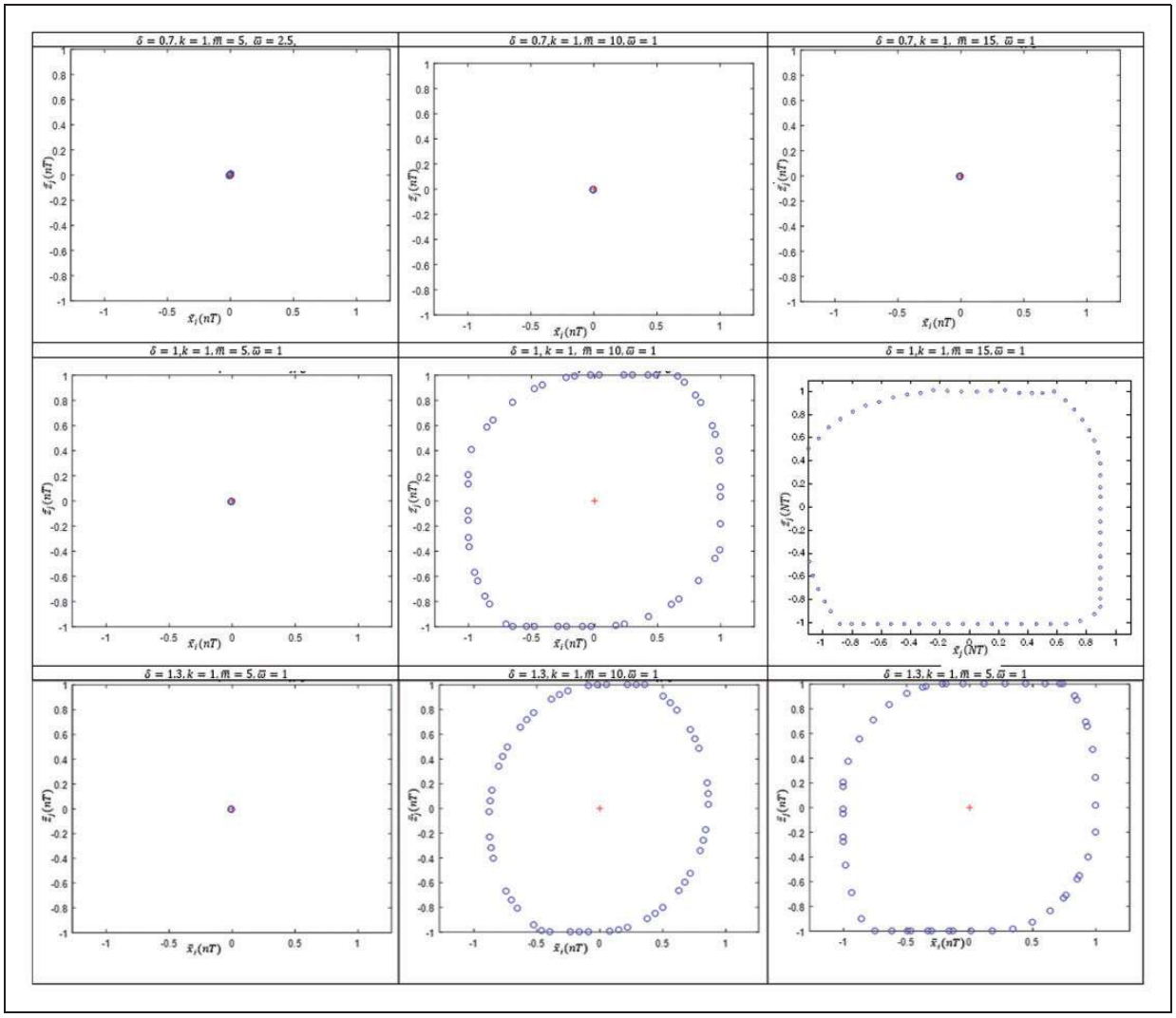

Figure 8. Poincaré map two-lobe bearing.

yields the bifurcation of the rotor centre for the range of speed $\bar{m} < 6.2$. For the dilatant lubricant ($k = 1.3$), bearing shows the bifurcation of the rotor centre for the speed range $\bar{m} < 5.9$. By taking non-dimensional journal speed, bifurcation map has been plotted in Figure 10 to visualize the influence of non-dimensional speed parameter on rotor bearing system behavior. The bearing operating with the dilatant lubricant shows a stable behavior and no unstable motion has been observed between $0 < \bar{\omega} < 3$, whereas the rotor bearing system operating with the pseudo-plastic lubricant also shows a stable behavior as compare to system operating with Newtonian lubricant. The pseudo-plastic lubricant $1.3 < \bar{\omega}$

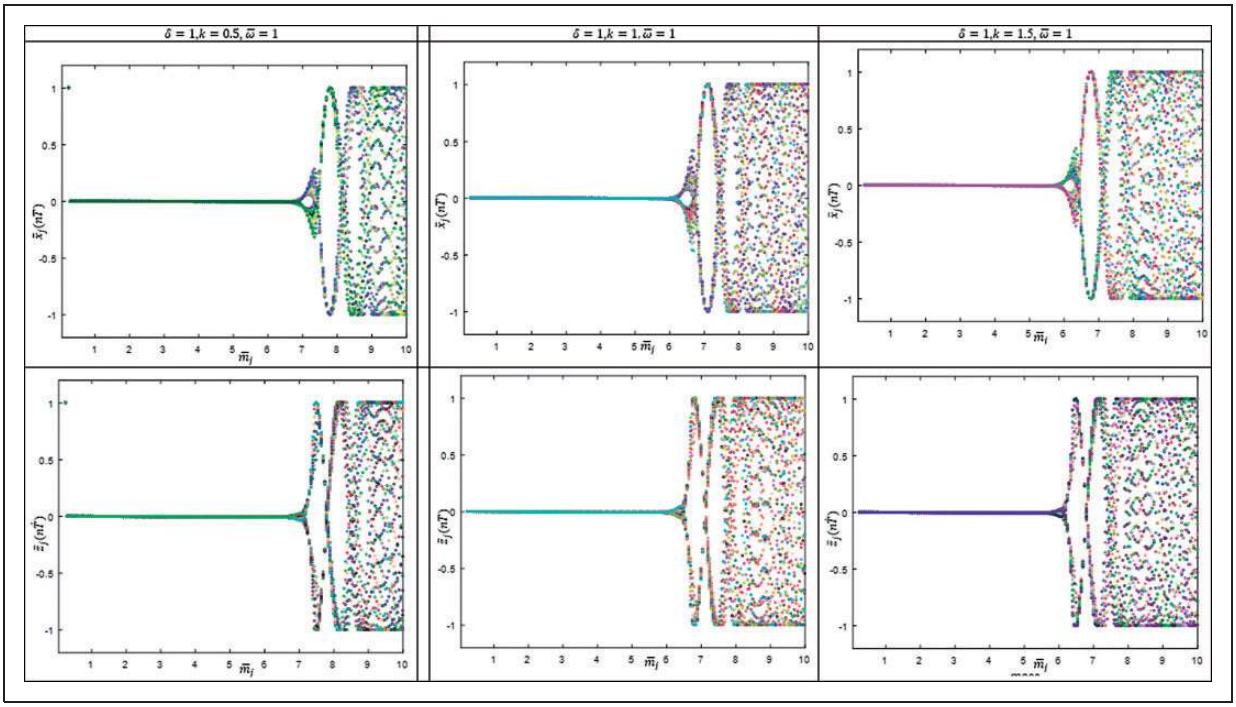

Figure 9. Bifurcation diagram of two-lobe bearing operating by taking mass as a system parameter.

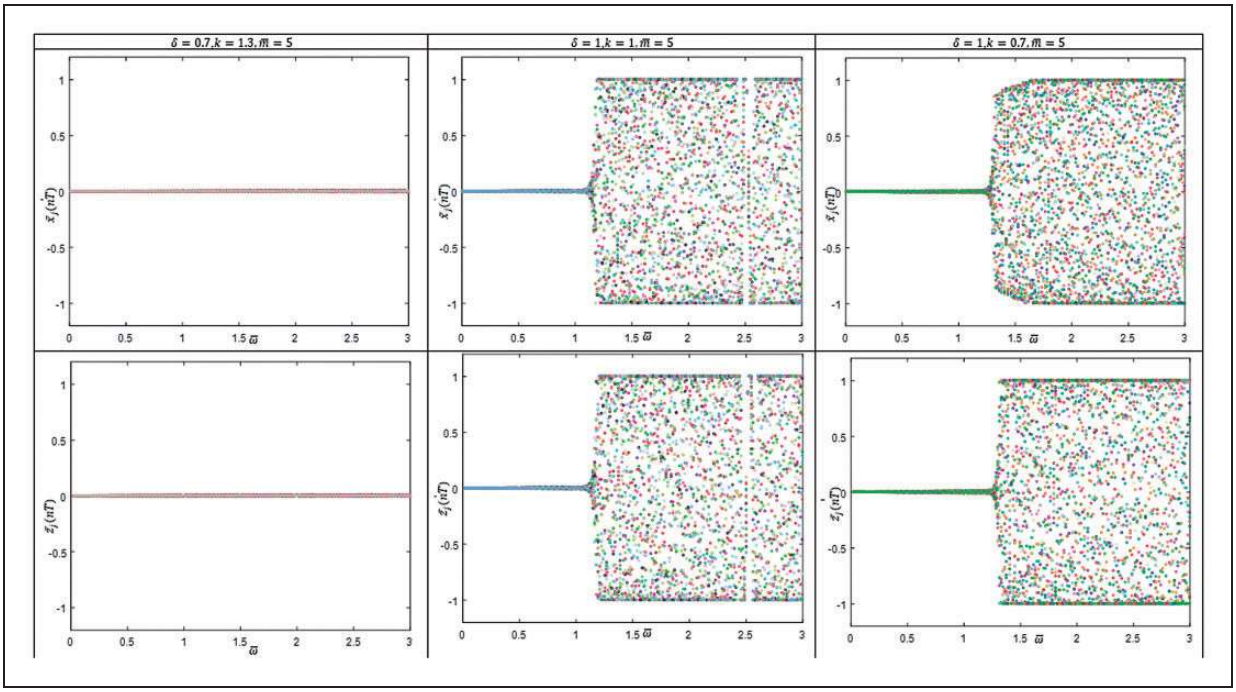

Figure 10. Bifurcation map of two-lobe bearing circular bearing operating with journal velocity.

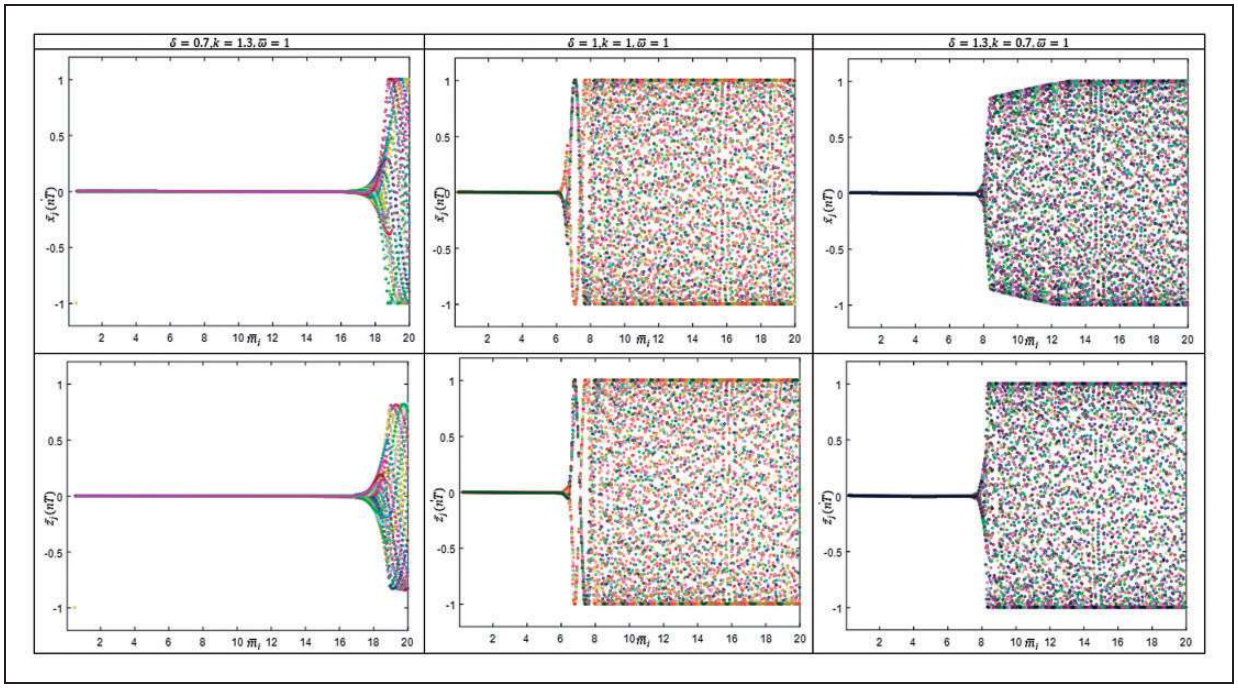

Figure 11. Bifurcation of two-lobe bearing circular bearing with mass.

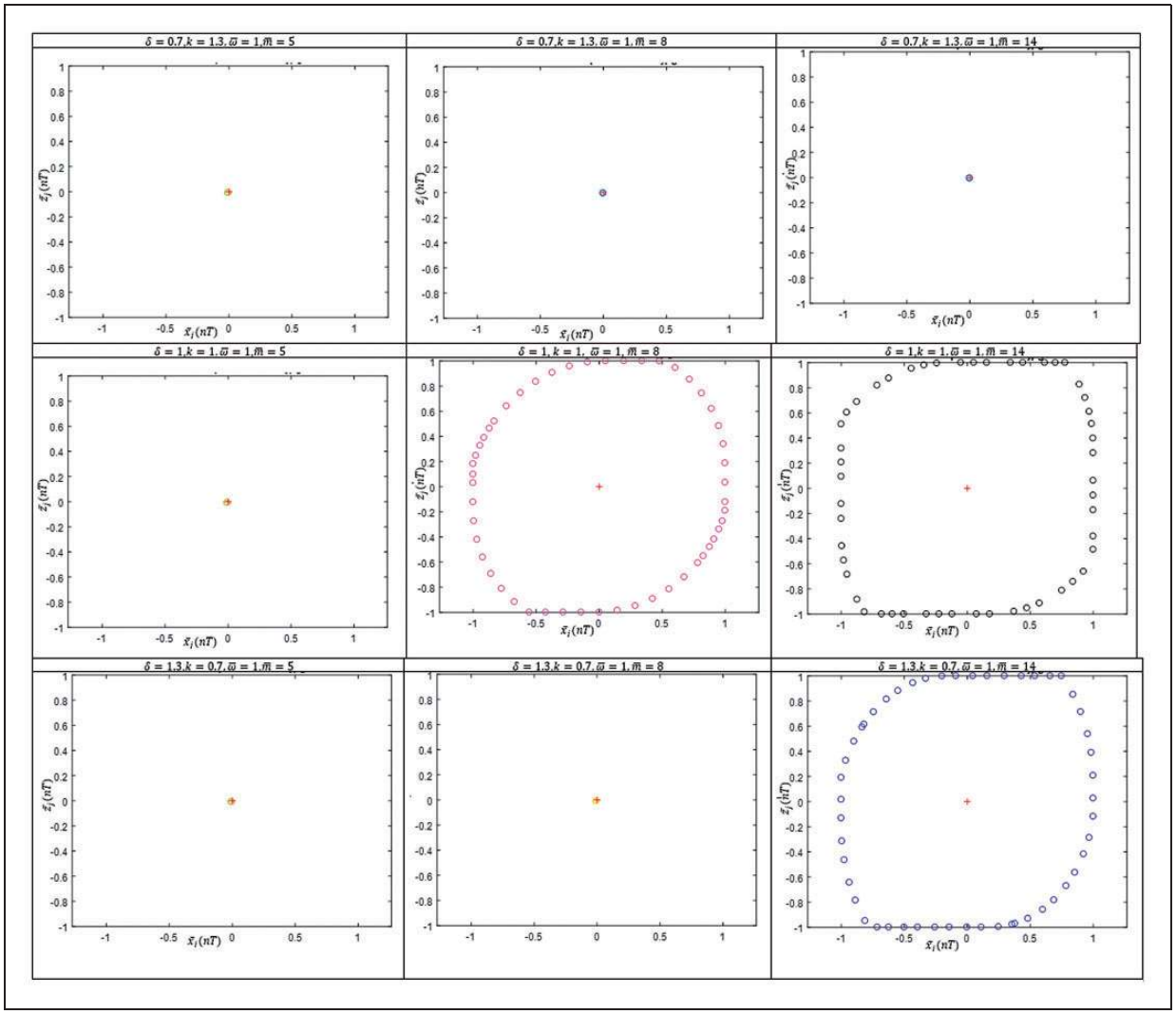

Figure 12. Poincaré map two-lobe bearing.

shows unstable behavior of the system. From Figure 10, it may be observed that non-Newtonian behavior results significantly change in the system behavior.

Combined effect of bearing ellipticity and non-Newtonian parameter

As discussed in an earlier section, great change in the system behavior has been observed as the bearing offset factor and lubricant behavior changes. Therefore, in this section, a study has been performed by taking combined effect of offset factor and non-Newtonian parameter. Figure 11 shows the effect of the bearing ellipticity on the bearing's stability. Bifurcation map in Figure 11 has been plotted by taking the non-dimensional rotor mass as a system parameter. Figure 11 shows a two-lobe bearing operating with the dilatant lubricant shows a stable behavior as compare to circular bearing operating with the Newtonian lubricant. Therefore, to get a stable design of system, a study has been done by taking the combined effect of bearing ellipticity and non-Newtonian parameter. The combined influences of offset factor of bearing and non-Newtonian parameter on the bearing's stability have also been studied. As shown in Figure 8, the bifurcation diagram of bearing is plotted by taking the different non-dimensional masses and ellipticity ratios. A significant improvement may be observed in the stability of the bearing by using the pseudo-plastic lubricant and bearing ellipticity effect. For the elliptical bearing at $\delta = 0.7$ and the pseudo-plastic lubricant at $k = 1.3$, the bifurcation of the journal center has been observed $\bar{m} > 17$. For the rotor bearing system at $\delta = 1$, i.e. circular bearing and for the Newtonian lubricant at $k = 1$, the bifurcation of the journal centre is shown for $\bar{m} > 6$. For the elliptical bearing ($\delta = 1.3$) and the pseudo-plastic lubricant ($k = 0.7$), the bifurcation of the journal center is observed for $\bar{m} > 8$. It may be noticed that to make the bearing stable, addition of additives can be useful instead of changing the bearing geometry. However, the effect of lubricant additives is small as compared to the effect of the bearing geometry.

To study dynamic periodic motion of the bearing, Poincaré map by taking the periodic data has been plotted in Figure 12 by taking different non-dimensional masses, ellipticity ratio to show the influence of non-dimensional mass on dynamic behavior. A stable motion has been recorded for $k = 1, \bar{m} = 5, \bar{\omega} = 1$ at all values of ellipticity ratios ($\delta = 0.7, 1.0, 1.3$) whereas unstable motions for ($\delta = 1$) have been observed at $k = 1, \bar{\omega} = 1$ and $\bar{m} < 8$. Bearing operating with the dilatant lubricant is more stable. Figure 12 indicates that for a small change in mass of the system results in a significant change in the stability of the system. By changing the lubricant behavior and bearing ellipticity, the dynamic behavior of completely changes.

Conclusion

Understanding of bearing characteristics is vital for the configuration of machine components in engineering applications. In the previous section, the effect of bearing geometry and lubricant behavior discussed on the system performance. The stability of the rotating system is an integral function of design of the fluid film journal bearings. The results present the bifurcation maps of a rigid rotor supported by a two-lobe fluid bearing operating with the non-Newtonian lubricant. The present work shows dynamic behavior of a rotordynamic system with the non-Newtonian lubricant. The non-Newtonian lubricant significantly changes the system behavior. Bifurcation diagram has been plotted by taking rotor mass and rotor speed as system parameters. On the basis of results and discussion, the following conclusions are drawn.

1. Non-Newtonian behavior of bearing also results in the stability of the bearing. Pseudo-plastic behavior of the lubricant makes the bearing more stable, whereas dilatant behavior of the lubricant results in decrease of the bearing's stability.
2. The stability of the system is an integral function of the bearing geometry and lubricant behavior. The stability in the system can be achieved, if the lubricant and geometry is properly chosen.
3. A significant improvement in the dynamic stability of the bearing is observed if the proper combination of non-Newtonian parameter and bearing offset ratio is used. As the bearing operating with the dilatant lubricant is more stable.

$$stability\big|_{(k=1.3,\delta=0.7)} > stability\big|_{(k=1,\delta=0.7)} > stability\big|_{(k=0.7,\delta=1.3)}$$

$$stability\big|_{(\delta=0.7)} > stability\big|_{(\delta=1)} > stability\big|_{(\delta=1.3)}$$

$$stability\big|_{(k=1.3)} > stability\big|_{(k=1)} > stability\big|_{(k=0.7)}$$

4. The results developed in this study will help bearing designer to avoid undesirable behavior of rotor center trajectory and bearing center trajectory, hence life of rotor system will increase.

Declaration of Conflicting Interests

The author(s) declared no potential conflicts of interest with respect to the research, authorship, and/or publication of this article.

Funding

The author(s) received no financial support for the research, authorship, and/or publication of this article.

ORCID iD

Arvind K Rajput http://orcid.org/0000-0002-6905-1928

References

1. Adiletta G, Guido AR and Rossi C. Chaotic motions of a rigid rotor in short journal bearings. *Nonlinear Dyn* 1996; 10: 251–269.
2. Miura T, Inoue T and Kano H. Nonlinear analysis of bifurcation phenomenon for a simple flexible rotor system supported by a full-circular journal bearing. *J Vib Acoust* 2017; 139: 031012.
3. Mongkolcheep K, Ruimi A and Palazzolo A. Modal reduction technique for predicting the onset of chaotic behavior due to lateral vibrations in drillstrings. *J Vib Acoust* 2015; 137: 021003.
4. Wang C-C and Chen C-K. Bifurcation analysis of self-acting gas journal bearings. *J Tribol* 2001; 123: 755–767.
5. Chang-Jian C-W and Chen C-K. Chaos and bifurcation of a flexible rub-impact rotor supported by oil film bearings with nonlinear suspension. *Mech Mach Theory* 2007; 42: 312–333.
6. Wang C-C. Bifurcation analysis of an aerodynamic journal bearing system considering the effect of stationary herringbone grooves. *Chaos Solitons Fractals* 2007; 33: 1532–1545.
7. Wang C-C, Yau H-T, Jang M-J, et al. Theoretical analysis of the non-linear behavior of a flexible rotor supported by herringbone grooved gas journal bearings. *Tribol Int* 2007; 40: 533–541.
8. Wang C-C. Theoretical and nonlinear behavior analysis of a flexible rotor supported by a relative short herringbone-grooved gas journal-bearing system. *Physica D* 2008; 237: 2282–2295.
9. Yang L-H, Wang W-M, Zhao S-Q, et al. A new nonlinear dynamic analysis method of rotor system supported by oil-film journal bearings. *Appl Math Model* 2014; 38: 5239–5255.
10. Chen C-L and Yau H-T. Chaos in the imbalance response of a flexible rotor supported by oil film bearings with non-linear suspension. *Nonlinear Dyn* 1998; 16: 71–90.
11. Piekos ES. *Numerical simulation of gas-lubricated journal bearings for microfabricated machines*. PhD Thesis, Massachusetts Institute of Technology, Cambridge, USA, 2000.
12. Chouchane M and Amamou A. Bifurcation of limit cycles in fluid film bearings. *Int J Non Linear Mech* 2011; 46: 1258–1264.
13. Weimin W, Lihua Y, Tiejun W, et al. Nonlinear dynamic coefficients prediction of journal bearings using partial derivative method. *Proc IMechE, Part J: J Engineering Tribology* 2012; 226: 328–339.
14. Meybodi RR, Mohammadi AK and Bakhtiari-Nejad F. Numerical analysis of a rigid rotor supported by aerodynamic four-lobe journal bearing system with mass unbalance. *Commun Nonlinear Sci Numer Simul* 2012; 17: 454–471.
15. Rashidi R, Karami mohammadi A and Bakhtiari nejad F. Bifurcation and nonlinear dynamic analysis of a rigid rotor supported by two-lobe noncircular gas-lubricated journal bearing system. *Nonlinear Dyn* 2010; 61: 783–802.
16. Sinhasan R and Sah PL. Static and dynamic performance characteristics of an orifice compensated hydrostatic journal bearing with non-Newtonian lubricants. *Tribol Int* 1996; 29: 515–526.
17. Kushare PB and Sharma SC. Nonlinear transient stability study of two lobe symmetric hole entry worn hybrid journal bearing operating with non-Newtonian lubricant. *Tribol Int* 2014; 69: 84–101.
18. Sharma SC and Yadav SK. A comparative study of full and partial textured hybrid orifice compensated circular thrust pad bearing system. *Tribol Int* 2016; 95: 170–180.
19. Sharma SC and Yadav SK. Performance analysis of a fully textured hybrid circular thrust pad bearing system operating with non-Newtonian lubricant. *Tribol Int* 2014; 77: 50–64.
20. Dowson D. A generalized Reynolds equation for fluid-film lubrication. *Int J Mech Sci* 1962; 4: 159–170.
21. Sharma SC and Yadav SK. Performance of hydrostatic circular thrust pad bearing operating with Rabinowitsch fluid model. *Proc IMechE, Part J: J Engineering Tribology* 2013; 227: 1272–1284.
22. Kushare PB and Sharma SC. A study of two lobe non recessed worn journal bearing operating with non-Newtonian lubricant. *Proc IMechE, Part J: J Engineering Tribology* 2013; 227: 1418–1437.
23. Tayal SP, Sinhasan R and Singh DV. Analysis of hydrodynamic journal bearings with non-newtonian power law lubricants by the finite element method. *Wear* 1981; 71: 15–27.
24. Yadav SK, Rajput AK, Ram N, et al. A direct numerical approach to compute the nonlinear rotordynamic coefficient of the noncircular gas journal bearing. *Proc IMechE, Part J: J Engineering Tribology* 2018; 232: 453–468.
25. Holster PL and Jacobs JAH. Theoretical analysis and experimental verification on the static properties of externally pressurized air-bearing pads with load compensation. *Tribol Int* 1987; 20: 276–289.
26. Dhatt G, Lefrançois E and Touzot G. *Finite element method*. Hoboken: John Wiley & Sons, 2012.
27. Rajput AK, Yadav SK and Sharma SC. Effect of geometrical irregularities on the performance of a misaligned hybrid journal bearing compensated with membrane restrictor. *Tribol Int* 2017; 115: 619–627.
28. Awasthi RK, Jain SC and Sharma SC. Finite element analysis of orifice-compensated multiple hole-entry worn hybrid journal bearing. *Finite Elem Anal Des* 2006; 42: 1291–1303.
29. Yadav SK and Sharma SC. Finite element analysis of tilted thrust pad bearings of various recesses shapes considering thrust pad flexibility. *Proc IMechE, Part J: J Engineering Tribology* 2015; 230: 872–893.
30. Chen WJ and Gunter EJ. *Introduction to dynamics of rotor-bearing systems*. Victoria: Trafford, 2007.
31. Butcher JC. *The numerical analysis of ordinary differential equations: Runge–Kutta and general linear methods*. New York: Wiley-Interscience, 1987.
32. Rahmatabadi A, Nekoeimehr M and Rashidi R. Micropolar lubricant effects on the performance of noncircular lobed bearings. *Tribol Int* 2010; 43: 404–413.
33. Lund J and Thomsen K. A calculation method and data for the dynamic coefficients of oil-lubricated journal bearings. *Topics in fluid film bearing and rotor bearing system design and optimization*. 1978.
34. Lund J. Stability and damped critical speeds of a flexible rotor in fluid-film bearings. *J Manuf Sci Eng* 1974; 96: 509–517.

35. Jiang H, Chong ASE, Ueda Y, et al. Grazing-induced bifurcations in impact oscillators with elastic and rigid constraints. *Int J Mech Sci* 2017; 127: 204–214.

Appendix

Notation

A	area, m^2
$C_{x,y}$	fluid film damping coefficient, $\frac{Ns}{m}$
F_R	resultant fluid film reaction force $\sqrt{F_{rx}^2 + F_{ry}^2}$
F_e	external force (N)
h	local fluid film thickness, m
c	radial clearance in the horizontal direction when rotor is in the center, m
c_m	radial clearance in the vertical direction, m
p	fluid film pressure, N/m^2
p_s, p_a	ambient/atmospheric pressure, N/m^2
Q	bearing flow, m^3/s
n	total number of nodes in domain
n_t	total number of elements
$S_{x,z}$	fluid film stiffness coefficient, N/m
R	radius of journal/rotor, m
M_j	mass of the journal/rotor, kg
k_1, k_2, k_3, k_4	slope in Rung–Kutta method
k	non-Newtonian parameter of lubricant
x_j, z_j	coordinates of journal/rotor center
T	time period of complete cycle
t	time, s
δ	offset ratio, $\frac{c_m}{c}$
μ	lubricant viscosity, $Pa - s$
ρ	density of the lubricant, kg/m^3
λ	aspect ratio $\lambda = L/D$

Non-dimensional parameters

$\bar{C}_{x,z}$	$C_{x,z} \times \frac{c\omega}{R^2 p_s}$
$\bar{F}_R$	$\frac{F_R}{R^2 p_s}$
$\bar{F}_{rx}$	$\frac{F_{rx}}{R^2 p_s}$
$\bar{F}_{rz}$	$\frac{F_{rz}}{R^2 p_s}$
$\bar{h}$	$\frac{h}{c}$
$\dot{\bar{h}}$	$\frac{\partial \bar{h}}{\partial \tau}$
$\dot{\bar{x}}_j$	$\frac{\partial \bar{x}_j}{\partial \tau}$
$\dot{\bar{z}}_j$	$\frac{\partial \bar{z}_j}{\partial \tau}$
$\bar{p}$	$\frac{p}{p_s}$
$\bar{Q}$	$\frac{\mu}{p_s h_r^3} Q$
$\bar{M}_j$	$M_j \times \frac{mc\omega^2}{p_a R^2}$
$\bar{S}_{x,z}$	$S_{x,z} \times \frac{c}{R^2 p_s}$
$\bar{\omega}$	$\frac{R^2 \mu \omega}{p_s \times c^2}$
α	$\frac{X}{R}$
β	$\frac{Y}{R}$
τ	$t\omega$
$\bar{\mu}$	μ

Subscripts and superscripts

b	bearing
e	e^{th} element
0	steady state condition
N	time internal level
–	dimensionless parameter